BIOCHEMISTRY
## including biophysical chemistry & molecular biology

Interrogation of the Substrate Profile and Catalytic Properties of the Phosphotriesterase from *Sphingobium* sp. Strain TCM1: An Enzyme Capable of Hydrolyzing Organophosphate Flame Retardants and Plasticizers

Dao Feng Xiang,[†] Andrew N. Bigley,[†] Zhongjie Ren,[‡] Haoran Xue,[†,§] Kenneth G. Hull,[†,§] Daniel Romo,[†,§] and Frank M. Raushel*,[†,‡]

[†]Department of Chemistry, Texas A&M University, College Station, Texas 77843, United States
[‡]Department of Biochemistry & Biophysics, Texas A&M University, College Station, Texas 77843, United States

ABSTRACT: The most familiar organophosphorus compounds are the neurotoxic insecticides and nerve agents. A related group of organophosphorus compounds, the phosphotriester plasticizers and flame retardants, has recently become widely used. Unlike the neurotoxic phosphotriesters, the plasticizers and flame retardants lack an easily hydrolyzable bond. While the hydrolysis of the neurotoxic organophosphates by phosphotriesterase enzymes is well-known, the lack of a labile bond in the flame retardants and plasticizers renders them inert to typical phosphotriesterases. A phosphotriesterase from *Sphingobium* sp. strain TCM1 (*Sb*-PTE) has recently been reported to catalyze the hydrolysis of organophosphorus flame retardants. This enzyme has now been expressed in *Escherichia coli*, and the activity with a wide variety of organophosphorus substrates has been characterized and compared to the activity of the well-known phosphotriesterase from *Pseudomonas diminuta* (*Pd*-PTE). Structure prediction suggests that *Sb*-PTE has a β-propeller fold, and homology modeling has identified a potential mononuclear manganese binding site. *Sb*-PTE exhibits catalytic activity against typical phosphotriesterase substrates such as paraoxon, but unlike *Pd*-PTE, *Sb*-PTE is also able to effectively hydrolyze flame retardants, plasticizers, and industrial solvents. *Sb*-PTE can hydrolyze both phosphorus−oxygen bonds and phosphorus−sulfur bonds, but not phosphorus−nitrogen bonds. The best substrate for *Sb*-PTE is the flame retardant triphenyl phosphate with a k_{cat}/K_m of 1.7×10^6 M^{-1} s^{-1}. Quite remarkably, *Sb*-PTE is also able to hydrolyze phosphotriesters with simple alcohol leaving groups such as tributyl phosphate ($k_{cat}/K_m = 40$ M^{-1} s^{-1}), suggesting that this enzyme could be useful for the bioremediation of a wide variety of organophosphorus compounds.
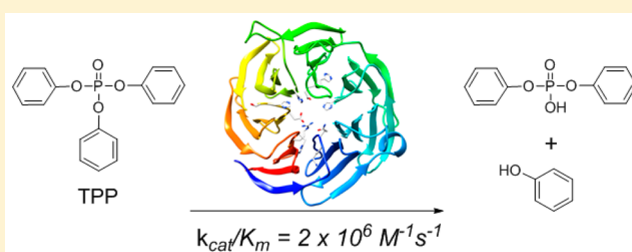
The most well-known organophosphates are the neurotoxic nerve agents and insecticides such as paraoxon (compound **1** in Scheme 1). These compounds are phosphotriesters, which inhibit the neural enzyme acetylcholine esterase by the enzymatic cleavage of a labile ester bond.[1] In recent years, a related group of organophosphotriesters has gained popularity for use as plasticizers and flame retardants in lubricants, durable plastics, and foams.[2,3] Compounds such as tris(2-chloroethyl) phosphate (**2**) and triphenyl phosphate (**3**), unlike the neurotoxic organophosphates, do not contain a labile ester bond but rather make use of the stable nature of these compounds to inhibit combustion and improve the performance of other organic compounds (Scheme 1). While not neurotoxins, many of the flame retardants contain halogenated alkyl or aromatic esters and are known, or suspected, chemical carcinogens.[3] These compounds are currently being utilized at rates of hundreds of metric tons per year.[2,3] The contamination of the environment by organophosphorus flame retardants has become widespread, and these compounds are now considered to be major emerging pollutants.[3]

Phosphotriesterases from bacteria such as *Pseudomonas diminuta* (*Pd*-PTE) and *Agrobacterium radiobacter* (OpdA) are well-known for their ability to hydrolyze and detoxify the neurotoxic organophosphates, but because of the lack of a sufficiently labile leaving group, these enzymes have little or no activity against the organophosphorus flame retardants and plasticizers.[4−9] Two novel phosphotriesterase-like enzymes from *Sphingomonas* sp. strain TDK1 (*Sm*-PTE) and *Sphingobium* sp. strain TCM1 (*Sb*-PTE) have recently been reported to hydrolyze organophosphates that are not substrates for other phosphotriesterases, such as *Pd*-PTE or OpdA.[10] Very little is known about these enzymes aside from their amino acid sequence and their dependence on the addition of divalent metal ions for catalytic activity. Currently, there is no structural or mechanistic information available for either *Sm*-PTE or *Sb*-PTE, or any close homologue of known function. In an effort to more clearly understand how these bacterial enzymes are able

Scheme 1
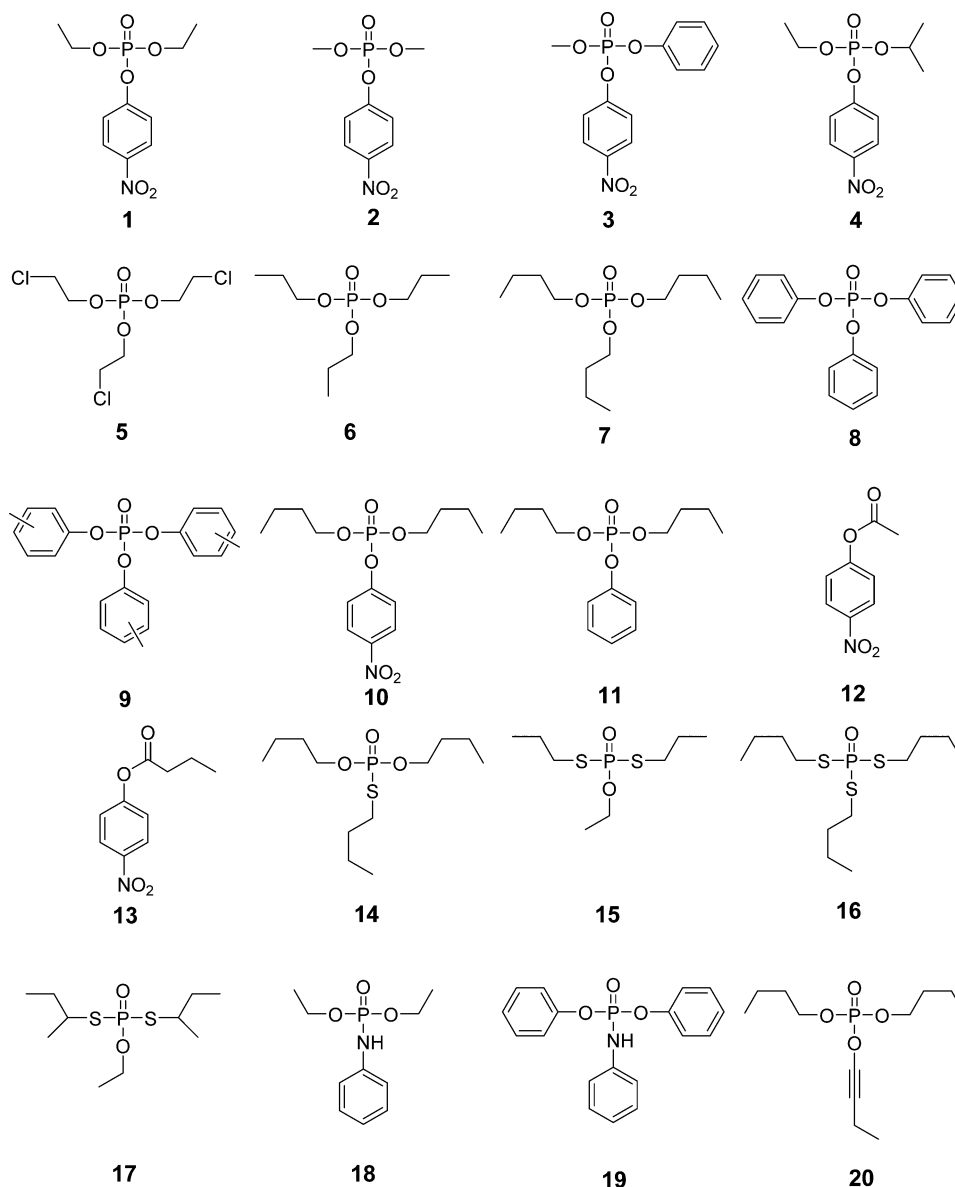
to efficiently hydrolyze organophosphates that lack a labile ester group, the gene for *Sb*-PTE was chemically synthesized and expressed in *Escherichia coli*. The substrate profile of *Sb*-PTE was determined, and a mechanism-based inhibitor was synthesized and subsequently shown to rapidly inactivate the catalytic properties of this enzyme. A sequence-based homology model of the *Sb*-PTE structure has been constructed, and a potential metal binding site has been identified.

■ MATERIALS AND METHODS

Materials. Unless otherwise noted, the bacterial growth medium was obtained from Research Products International and general chemicals were purchased from Sigma/Aldrich. Paraoxon (**1**), methyl paraoxon (**2**), tris(2-chloroethyl) phosphate (**5**), tripropyl phosphate (**6**), tributyl phosphate (**7**), triphenyl phosphate (**8**), tricresyl phosphate (**9**), 4-nitrophenyl acetate (**12**), 4-nitrophenyl butyrate (**13**), ethoprophos (**15**), tribufos (**16**), and cadusafos (**17**) were from Sigma-Aldrich. Methyl phenyl 4-nitrophenyl phosphate (**3**), ethyl isopropyl 4-nitrophenyl phosphate (**4**), and dibutyl

phenyl phosphate (**11**) were synthesized as previously reported.[11,12] Dibutyl 4-nitrophenylphosphate (**10**) was a gift from Lawrence Livermore National Laboratory. Wild-type *Pd*-PTE was expressed and purified as previously reported.[13]

Cloning and Expression of *Sb*-PTE. The reported protein sequence of *Sb*-PTE (gi|664819019) was used for the design of a chemically synthesized codon-optimized gene by GenScript (Piscataway, NJ) that was subsequently used for production of the enzyme in *E. coli*. The gene was subcloned into a pET30a (+) plasmid (EMD Millipore) using the NdeI and XhoI restriction sites for expression with a C-terminal His tag. The final construct was transformed into BL21(DE3) cells (EMD Millipore), and single colonies were used to inoculate 6 mL cultures of LB, which were grown for 9 h at 37 °C. The 6 mL cultures were subsequently used to inoculate 1 L cultures of Terrific Broth supplemented with 1.0 mM MnAc$_2$ and then grown at 30 °C for 14 h. The temperature was decreased to room temperature and growth continued for an additional 4–6 h. The optimal growth time was determined by tracking paraoxonase activity from the crude cell lysate. Once optimal

catalytic activity had been achieved, the cells were harvested by centrifugation and stored at −80 °C prior to purification of the enzyme.

Purification of *Sb*-PTE. Cell pellets (~10 g) were resuspended in 50 mL of binding buffer [20 mM HEPES (pH 7.9), 0.50 M NaCl, and 10 mM imidazole] and then disrupted by sonication using a Branson Sonifier 450. The cell lysate was clarified by centrifugation before being passed through a 0.22 μM syringe filter (VWR) and then loaded onto a 5 mL HisTrap HP column (GE Healthcare) attached to an NGC liquid chromatography system (Bio-Rad) previously equilibrated with binding buffer. The His-tagged protein was eluted with a 0 to 50% gradient with elution buffer [20 mM HEPES (pH 7.9), 0.25 M NaCl, and 0.50 M imidazole]. The fractions with paraoxonase activity were combined and concentrated. The buffer was exchanged using a PD-10 desalting column (GE Healthcare) equilibrated with 20 mM HEPES (pH 8.0). The final protein solution was brought to 100 mM NaCl to maintain protein stability. Protein purity was judged to be >95%, based on sodium dodecyl sulfate–polyacrylamide gel electrophoresis (SDS–PAGE). Protein identity was verified by N-terminal sequencing at the Protein Chemistry Laboratory at Texas A&M University. All metal analyses were conducted with nitric acid-hydrolyzed samples via ICP-MS at the Elemental Analysis Laboratory at Texas A&M University.

Mutagenesis. The gene for *Sb*-PTE was mutated at different residue positions using the QuikChange site-directed mutagenesis method from Agilent Technologies. The entire gene was subsequently sequenced for each mutant to ensure that there were no unwanted mutations, deletions, or insertions occurring during the process of mutagenesis. The mutant proteins were expressed in the presence of 1.0 mM MnCl$_2$ and then purified to homogeneity using the same procedure that was used for wild-type *Sb*-PTE.

Determination of the Optimal Metal for *Sb*-PTE. A 6 mL culture of BL21(DE3) cells containing the plasmid for expression of *Sb*-PTE was used to inoculate 1 L of Terrific Broth without a metal supplement, and the cultures were grown for 18 h at 30 °C. Samples (1.0 mL) were harvested via centrifugation, and the cells were lysed with Bug Buster (EMD Millipore). The lysates were filtered through a 0.22 μm syringe filter (VWR). Catalytic activity was assessed by adding 10 μL of lysate to a 250 μL reaction vessel containing 50 mM CHES (pH 9.0) and 1.0 mM paraoxon. Catalytic activity was measured in the presence or absence of 0.1 or 1.0 mM Ca^{2+}, Cd^{2+}, Co^{2+}, Zn^{2+}, or Mn^{2+}. All metal ions were added as chloride salts.

Measurement of Catalytic Activity. Enzymatic activities with compounds **1−4** and **8−11** were measured in a volume of 250 μL in 50 mM CHES (pH 9.0) using a Molecular Devices SpectraMax 384 Plus 96-well plate reader. Hydrolyses of paraoxon (**1**), dibutyl *p*-nitrophenyl phosphate (**10**), and compounds **2−4**, **12**, and **13** were followed by the release of *p*-nitrophenol (ΔE_{400} = 17000 M^{-1} cm^{-1}). Triphenyl phosphate (**8**) and dibutyl phenylphosphate (**11**) were followed by release of phenol at 270 nm (ΔE_{270} = 1240 M^{-1} cm^{-1}). The release of methyl phenol from tricresyl phosphate (**9**) hydrolysis was followed at 272 nm (ΔE_{272} = 2000 M^{-1} s^{-1}). Assays with compounds **3**, **10**, and **11** contained 10% methanol, while compounds **8** and **9** contained 20% methanol. The hydrolysis of compounds **18** and **19** was followed by the release of aniline (ΔE_{280} = 1300 M^{-1} cm^{-1}) in assays containing 50

mM CHES (pH 9.0) and 10% DMSO. Hydrolysis of compounds **14−17** was assayed at 30 °C in 250 μL reaction mixtures with 50 mM HEPES (pH 8.0), 1.0 mM MnCl$_2$, and 10% methanol, and the reactions were followed by the release of the thiol leaving group by the inclusion of 0.3 mM DTNB (ΔE_{412} = 14150 M^{-1} cm^{-1}).

The hydrolysis of compounds **5−7** was followed using a pH sensitive colorometric assay in 96-well format as previously described.[14,15] Briefly, protons released during hydrolysis were quantified by inclusion of 0.1 mM cresol purple in assays containing 2.5 mM BICINE (pH 8.3), 200 mM NaCl, and 5% DMSO. Cresol purple was added from a concentrated stock solution in DMSO. Reactions were monitored at 577 nm. The effective extinction coefficient (ΔE_{577} = 1680 M^{-1} s^{-1}) for cresol purple under these conditions was determined by the construction of a standard curve under the same reaction conditions with acetic acid as the proton donor. The kinetic constants were determined by fitting the data to the Michaelis–Menten equation.[16]

Synthesis of Dibutyl, Butylphosphorothiolate. Dibutyl, butylphosphorothiolate (**14**) was synthesized by following the reported procedure with modifications.[17,18] To a stirred solution of dibutyl phosphite (4.86 g, 0.025 mol, 1.0 equiv) in diethyl ether (20 mL) was added powdered sulfur (0.88 g, 0.0275 mol, 1.1 equiv) in 1 portion at ambient temperature (21 °C). Triethylamine (2.8 mL, 0.0275 mol, 1.1 equiv) was added slowly over 3 min, and the reaction mixture was stirred for 22 h. The reaction mixture was diluted with diethyl ether (100 mL) and washed with aqueous HCl (1.0 M, 30 mL). The organic phase was separated, dried over anhydrous MgSO$_4$, and concentrated *in vacuo*. The crude *O,O*-dibutyl phosphorothioic acid (6.5 g) was used in the next step without further purification.

To a stirred solution of *O,O*-dibutyl phosphorothioic acid (prepared as described above, 500 mg, ~2.21 mmol) in anhydrous toluene (6 mL) were added triphenylphosphine (580 mg, 2.21 mmol, 1.0 equiv) and *n*-butanol (0.22 mL, 2.43 mmol, 1.1 equiv). Diisopropyl azodicarboxylate (DIAD, 0.44 mL, 2.23 mmol, 1.0 equiv) was then added, and the reaction mixture was heated at 35 °C for 2 h. The reaction mixture was cooled to ambient temperature (21 °C) and filtered, and the solid was washed with toluene (2 × 5 mL). The filtrate was combined and concentrated *in vacuo*, and the residue was purified by silica gel column chromatography (1/20 to 1/5 acetone/hexanes) to give *O,O,S*-tributyl phosphorothioate (345 mg, 55%) as a colorless oil: ^{1}H NMR (500 MHz, CDCl$_3$) δ 4.25−3.72 (m, 4H), 2.76 (dt, *J* = 7.3, 14.0 Hz, 2H), 1.70−1.53 (m, 6H), 1.43−1.28 (m, 6H), 0.87 (t, *J* = 7.4 Hz, 6H), 0.85 (t, *J* = 7.4 Hz, 3H); ^{13}C NMR (125 MHz, CDCl$_3$) δ 66.9 (d, $^3J_{C-P}$ = 6.3 Hz), 32.7 (d, $^4J_{C-P}$ = 5.6 Hz), 32.0 (d, $^3J_{C-P}$ = 7.4 Hz), 30.4 (d, $^4J_{C-P}$ = 3.9 Hz), 21.5, 18.6, 13.4, 13.3; ^{31}P{^{1}H} NMR (121 MHz, CDCl$_3$) δ 29.2 (s); high-resolution MS (ESI) calcd for C$_{12}$H$_{28}$O$_3$PS$^+$ [M + H]$^+$ 283.1497, found 283.1495.

Synthesis of 1-Butynyl Dibutylphosphate. 1-Butynyl dibutylphosphate (**20**) was synthesized according to the method of Stang.[19] To an ice-cold suspension of iodosobenzene (591 mg, 2.68 mmol) and but-1-yn-1-yltrimethylsilane (422 mg, 3.35 mmol) in chloroform (7.0 mL) was slowly added BF$_3$·OEt$_2$ (0.34 mL, 2.68 mmol).[20,21] The mixture was allowed to warm to ambient temperature (21 °C), stirred for 3 h, and then recooled to 0 °C. In a separate flask, dibutyl phosphate (2.66 mL, 13.4 mmol) was mixed with a solution of 10% NaOH at 0 °C. The mixture was stirred for 1 h and then added

to the organic solution prepared as described above. The mixture was stirred vigorously for 5 min and separated, and then the aqueous phase was extracted with CHCl$_3$ (3 × 10 mL). The combined organic layers were washed with brine, dried over anhydrous MgSO$_4$, and then concentrated *in vacuo*. The residue was dissolved in anhydrous CH$_2$Cl$_2$ (17 mL) at ambient temperature (21 °C) and stirred for 16 h. After concentration, the residue was purified by silica gel column chromatography (4/1 hexanes/ethyl acetate) to give 1-butynyl dibutyl phosphate (128 mg, 18%) as a light yellow oil: ^{1}H NMR (300 MHz, C$_6$D$_6$) δ 3.99 (m, 4H), 1.93 (qd, J = 7.5, 3.5 Hz, 2H), 1.49−1.27 (m, 4H), 1.24−1.03 (m, 4H), 0.93 (t, J = 7.5 Hz, 3H), 0.69 (t, J = 7.3 Hz, 6H); ^{31}P{^{1}H} NMR (121 MHz, C$_6$D$_6$) δ −3.63 (s); ^{13}C NMR (75 MHz, C$_6$D$_6$) δ 80.5 (d, $^2J_{C-P}$ = 9.7 Hz), 69.3 (d, $^2J_{C-P}$ = 6.1 Hz), 41.1 (d, $^3J_{C-P}$ = 6.0 Hz), 32.3 (d, $^3J_{C-P}$ = 6.5 Hz), 18.7, 14.4, 13.5, 10.9; high-resolution MS (ESI) calcd for C$_{12}$H$_{24}$O$_4$P$^+$ [M + H]$^+$ 263.1412, found 263.1400.

Inactivation of *Sb*-PTE by 1-Butynyl Dibutylphosphate. To assess the interaction of *Sb*-PTE with 1-butynyl dibutylphosphate (**20**), the enzyme (32 nM) was mixed with this compound in various molar ratios ranging from 0 to 37.5 in 50 mM CHES buffer (pH 9.0). The residual catalytic activity of Sb-PTE was assayed using 0.40 mM paraoxon as the substrate. Samples of the fully inhibited enzyme were subjected to MS analysis to determine the number of modifications on the intact protein in the presence of excess inhibitor. For reactivation studies, 500 μL samples of the inhibited enzyme were prepared by mixing 1.3 μM enzyme with 30 μM 1-butynyl dibutylphosphate in 50 mM HEPES (pH 7.0). The enzyme was fully inhibited within 10 min. Reactivation of the inhibited enzyme was tested by diluting samples 1:2 into a reactivation mixture containing 50 mM CHES (pH 9.0) and hydroxylamine (0−20 mM). The reactivation of catalytic activity was followed over time by measuring the enzymatic activity using 0.60 mM paraoxon as the substrate. Reactivation of *Sb*-PTE was also examined, in the absence of added hydroxylamine, by variation of the pH from 7 to 10.

MS/MS Analysis of Inactivated *Sb*-PTE. Samples of *Sb*-PTE, which had been inactivated by 1-butynyl dibutylphosphate, and a control sample were loaded on SDS−PAGE gels at a concentration of 1.5 mg/mL and visualized by Coomassie Blue staining. The samples were proteolyzed via the addition of trypsin using a previously described protocol.[22] The samples were analyzed by LC−MS (Dionex nanoRSLC and an Orbitrap Fusion Tribrid Mass Spectrometer from Thermo Scientific). Briefly, 1.0 μL of the digested protein sample was loaded onto a 75 μm × 15 cm Acclaim Pepmap C18 column and eluted over 30 min with a total run time of 1 h. The eluted peptides were introduced into the mass spectrometer and analyzed using the Orbitrap (OT) mass spectrometer in positive ion mode with the following settings: resolution, 120 K; scan range, m/z 200−1800; maximal injection time, 50 ms; AGC target, 2 × 104; S-lens RF level, 60. Charge states ranging from 2 to 7 were accepted, and targeting ions were excluded for 60 s. MS/MS data were obtained using the HCD cell, and fragment masses were determined using the OT mass spectrometer at a resolution of 30 K. The data were analyzed using PEAKS Studio Software (Thermo Scientific). For the analysis of peptide MS and MS/MS from the inhibitor modification experiments, maximal mass deviations of 10 ppm for MS and 0.5 D for MS/MS were accepted. Additionally, carbamidomethylation of cysteine was taken into account as a fixed

modification, and oxidation of methionine was set as a varied modification. Up to three missed cleavage sites were utilized during data processing.

Construction of the *Sb*-PTE Homology Model. A protein BLAST was conducted using the sequence of *Sb*-PTE (gil664819019) to identify related proteins in the non-redundant protein sequence collection. The protein sequence for *Sb*-PTE was then submitted to numerous protein structure prediction servers. All of the highly rated protein structures were found to be seven-blade β-propeller folds. Homology models were built using the structure predictor servers Phyre2 and FFAS using the leptospiral antigen Lp49 protein from *Leptospira interrogans* [Protein Data Bank (PDB) entry 3BWS].[23−25] Structural alignment of the two structures was conducted using Chimera.[26]

Preparation of Apo and Mn-Reconstituted *Sb*-PTE. Buffers for metal chelation were made metal-free by being passed through Chelex 100 Resin (Bio-Rad). Samples of wild-type *Sb*-PTE and its variants at a concentration of 1.5 mg/mL were incubated with 2.0 mM EDTA in 50 mM MES (pH 6.0) and 100 mM NaCl for 18 h at 4 °C. Metal and excess EDTA were removed when the protein was passed through a PD-10 desalting column (GE-Healthcare) previously equilibrated with 50 mM metal-free MES (pH 8.0) with 100 mM NaCl. Protein was dialyzed against 50 mM metal-free HEPES (pH 8.0) with 100 mM NaCl. Metal analysis by ICP-MS showed no detectable metal, and the enzymatic activity was <0.1% of the as-purified protein. Reconstitution of enzyme activity was achieved by incubation of the protein at a concentration of 1 mg/mL with 100 equiv of MnCl$_2$ overnight.

■ RESULTS

Determination of the Optimal Metal for *Sb*-PTE. The first bacterial cultures used for the expression of *Sb*-PTE were grown without metal supplementation. Crude cell lysates of these cultures were subsequently tested for catalytic activity against the insecticide paraoxon (**1**). Various divalent metal ions were added to the assays, and the results are summarized in Figure 1. No activation was observed with the inclusion of zinc or calcium. A modest (∼2-fold) enhancement of catalytic activity was obtained with cadmium or cobalt. The largest
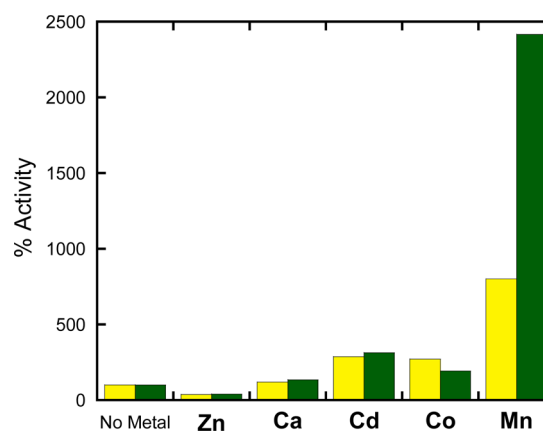

Figure 1. Activation of *Sb*-PTE in crude cell lysates by the addition of divalent metal ions directly to the assay mixtures. Yellow bars are for the addition of metal at a final concentration of 0.1 mM, and the green bars are for the addition of 1.0 mM metal. The enzyme activity was measured at pH 9.0 using 1.0 mM paraoxon as the substrate.
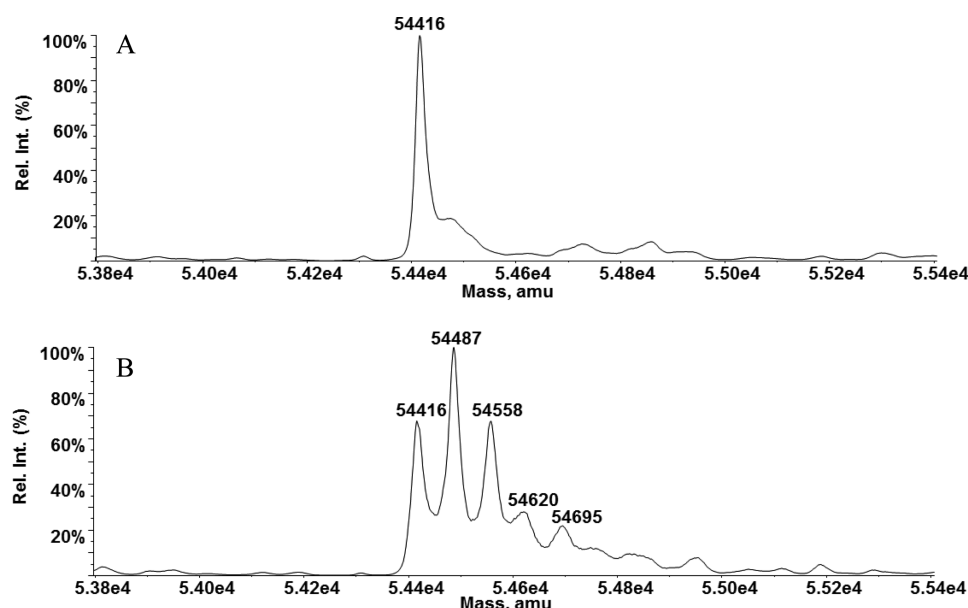
Figure 2. MS of (A) intact *Sb*-PTE and (B) 1-butynyl dibutylphosphate (**18**)-inactivated *Sb*-PTE. Masses of major species are listed with the labeled protein showing addition of up to four butyl groups.

Table 1. Kinetic Constants for *Sb*-PTE and *Pd*-PTE with Selected Substrates at 30 °C

| substrate	k_{cat} (s^{-1})	K_m (μM)	k_{cat}/K_m (M^{-1} s^{-1})
		Sb-PTE	
paraoxon (**1**)	28 ± 1	360 ± 20	(7.7 ± 0.5) × 10^4
methyl paraoxon (**2**)	1.7 ± 0.1	270 ± 30	(6.3 ± 0.7) × 10^3
methyl phenyl 4-nitrophenylphosphate (**3**)	2.1 ± 0.1	93 ± 8	(2.3 ± 0.2) × 10^4
ethyl propyl 4-nitrophenylphosphate (**4**)	1.90 ± 0.03	66 ± 7	(2.9 ± 0.3) × 10^4
tris(2-chloroethyl) phosphate (**5**)	0.60 ± 0.02	150 ± 20	(3.6 ± 0.4) × 10^3
tripropyl phosphate (**6**)	nd^a	nd^a	(1.7 ± 0.2) × 10
tributyl phosphate (**7**)	nd^a	nd^a	(3.9 ± 0.3) × 10
triphenyl phosphate (**8**)	57 ± 2	34 ± 3	(1.7 ± 0.2) × 10^6
tricresyl phosphate (**9**)	nd^a	nd^a	(6.2 ± 0.7) × 10^5
dibutyl 4-nitrophenyl phosphate (**10**)	5.9 ± 0.3	150 ± 20	(4.0 ± 0.4) × 10^4
dibutyl phenylphosphate (**11**)	3.7 ± 0.1	140 ± 10	(2.6 ± 0.2) × 10^4
4-nitrophenyl acetate (**12**)	nd^a	nd^a	(2.2 ± 01) × 10^3
4-nitrophenyl butyrate (**13**)	1.50 ± 0.06	0.30 ± 0.04	(5.0 ± 0.7) × 10^3
dibutyl butylphosphorothiolate (**14**)	0.34 ± 0.01	85 ± 8	(4.0 ± 0.4) × 10^3
ethoprophos (**15**)	nd^a	nd^a	(1.6 ± 0.1) × 10^3
S,S,S-tributyl phosphorotrithioate (**16**)	0.60 ± 0.02	25 ± 3	(2.4 ± 0.1) × 10^4
cadusafos (**17**)	nd^a	nd^a	(2.1 ± 0.1) × 10^3
diethyl analinephosphate (**18**)	nd^a	nd^a	<10^{-3}
diphenyl analinephosphate (**19**)	nd^a	nd^a	<10^{-3}
		Pd-PTE	
paraoxon (**1**)	2230 ± 40	140 ± 10	(2.4 ± 0.2) × 10^7
dibutyl p-nitrophenyl phosphate (**10**)	570 ± 40	380 ± 30	(1.5 ± 0.2) × 10^6
dibutyl phenyl phosphate (**11**)	nd^a	nd^a	(1.1 ± 0.1) × 10^0
triphenyl phosphate (**8**)	nd^a	nd^a	<10^{-3}

^{a}Not determined.

enhancement was observed with manganese, where an 8-fold enhancement was obtained at a concentration of 0.1 mM and a 25-fold enhancement was observed at 1.0 mM. All subsequent cultures and measurements of catalytic activity were supplemented with 1.0 mM manganese.

Protein Expression and Purification. Protein expression was optimized for catalytic activity in Terrific Broth using the protein fused with a C-terminal His tag to allow facile enzyme purification. After elution from the HisTrap HP (GE Health

Care) column, a single protein band was observed via SDS−PAGE; however, the estimated molecular mass of 54 kDa was somewhat smaller than the expected molecular mass for *Sb*-PTE (63.5 kDa) based on the amino acid sequence derived from the DNA sequence. To verify the identity of the purified protein, it was submitted for N-terminal amino acid sequencing. The N-terminal amino acid sequence of the purified protein was found to be QVVLG, which corresponds to residues 88−92 of *Sb*-PTE.[10] The expected mass of the protein lacking the first

Scheme 2
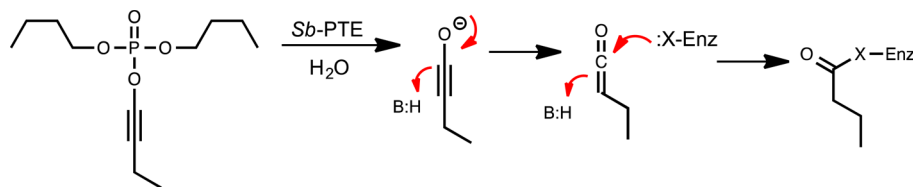
87 amino acids is 54422 Da. The purified protein was submitted for mass spectrometric analysis, and the molecular mass was found to be 54416 Da (Figure 2A). The previously reported mass for *Sb*-PTE, purified directly from *Sphingobium* sp. strain TCM1, was reported to be 58.6 kDa, suggesting that the native protein is cleaved in both *E. coli* and *Sphingobium* sp. strain TCM1.[10] The metal content of the purified *Sb*-PTE was determined to be 0.8 equiv of Mn^{2+} and 0.1 equiv of Zn^{2+} per protein subunit as measured by ICP-MS. Approximately 7−10 mg of *Sb*-PTE can be purified from each liter of cell culture.

Catalytic Properties. The kinetic constants for the hydrolysis of selected substrates by *Sb*-PTE were determined, and the results are listed in Table 1. For comparison, the kinetic constants for the hydrolysis for some of the same compounds by *Pd*-PTE were determined under identical reaction conditions. The catalytic efficiency for the hydrolysis of dibutyl *p*-nitrophenyl phosphate (**10**) by *Sb*-PTE is significant at 4×10^4 M^{-1} s^{-1}, but this value is approximately 2 orders of magnitude smaller than that exhibited by *Pd*-PTE. With the unactivated phenolate leaving group, the catalytic activity of *Pd*-PTE is diminished 10^6-fold for the hydrolysis of dibutyl phenyl phosphate (**11**), relative to that of dibutyl *p*-nitrophenyl phosphate (**10**). However, the catalytic activity for the hydrolysis of compound **11** is essentially the same as for the hydrolysis of compound **10** by *Sb*-PTE. Against the flame retardant triphenyl phosphate (**8**), *Pd*-PTE has no detectable activity, but the catalytic activity of *Sb*-PTE is increased to 1.7×10^6 M^{-1} s^{-1}. *Sb*-PTE can similarly hydrolyze the flame retardant tris(2-chloroethyl) phosphate (**5**) and the aviation fuel additive tricresol phosphate (**9**) with kinetic constants of 4×10^3 and 6×10^5 M^{-1} s^{-1}, respectively. *Sb*-PTE can hydrolyze the pesticides methyl paraoxon (**2**), ethoprophos (**15**), tribufos (**16**), and cadusafos (**17**) at similar rates. *Sb*-PTE was also found to hydrolyze the nerve agents methyl phenyl 4-nitrophenyl phosphate (**3**) and ethyl, isopropyl 4-nitrophenylphosphate (**4**) with rate constants in excess of 10^4 M^{-1} s^{-1}. *Sb*-PTE can hydrolyze the industrial solvents tributyl phosphate (**7**) and tripropyl phosphate (**6**) with rate constants of $<10^2$ M^{-1} s^{-1}. Introduction of a thiol linkage into dibutyl butylphosphorothiolate (**14**) or a 4-nitrophenyl group in dibutyl 4-nitrophenyl phosphate (**10**) improved activity by 2 or 3 orders of magnitude, respectively. *Sb*-PTE was also found to hydrolyze simple ester linkages in 4-nitropheyl acetate (**12**) and 4-nitrobutyrate (**13**) with activity similar to those of many of the phosphate triester substrates. The ability of *Sb*-PTE to hydrolyze phosphorus−nitrogen bonds was addressed using diethyl and diphenyl analinephosphate (**18** and **19**). With these compounds, no activity could be observed, suggesting that *Sb*-PTE is not able to hydrolyze phosphorus−nitrogen bonds.

Inactivation of *Sb*-Phosphotriesterase. 1-Butynyl dibutylphosphate (**20**) was synthesized and tested as a mechanism-based inactivator of *Sb*-PTE. The enzymatic hydrolysis of this compound is expected to generate a highly reactive ketene intermediate,[27] which can potentially react with available nucleophiles in the active site as illustrated in Scheme 2. The alkynyl phosphate ester was found to be a highly effective inhibitor of *Sb*-PTE with nearly complete inhibition achieved with near stoichiometric amounts of inhibitor (Figure 3). The
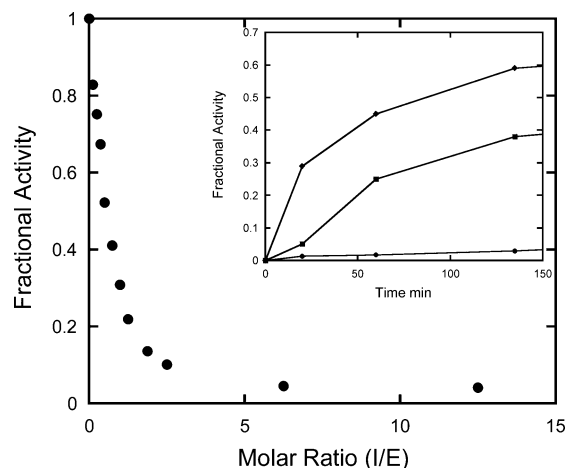

Figure 3. Inactivation of *Sb*-PTE by 1-butynyl dibutylphosphate (**18**). Various amounts of the mechanism-based inactivator **18** were added to 32 nM *Sb*-PTE in CHES buffer (pH 9.0). Aliquots were removed after 10 min and tested for catalytic activity using 0.40 mM paraoxon at pH 9.0. The inset shows the reactivation of enzyme activity after the addition of hydroxylamine [(●) 0, (■) 1.0, and (◆) 5.0 mM] at pH 7.0. The activity of the rescued enzyme was assayed with 0.6 mM paraoxon in 50 mM CHES (pH 9.0).

mass spectrum of the modified protein exhibited two major additional peaks that are shifted by ~71 and ~142 Da, relative to the unlabeled protein, and two minor peaks. This result is consistent with the addition of one and two ketene groups to the protein (Figure 2B).

Reactivation of the enzyme by the addition of hydroxylamine and changes in pH were attempted. Incubation of the inhibited enzyme with 5.0 mM hydroxylamine was found to restore approximately 60% of the enzymatic activity in 3 h, and >90% of the original catalytic activity was restored after 24 h. A similar reactivation profile occurs after incubation of the inhibited enzyme at pH 10 (data not shown). Analysis of the MS/MS spectra of the inhibited protein identified residues Tyr-219, Ser-474, Tyr-456, and Ser-458 as being modified by the mechanism-based inactivator (Figure 4).

The addition of the substrate reduced the rate of inactivation of *Sb*-PTE by the suicide substrate **20**. The ability of the substrate to protect the enzymatic activity was tested by changing the order of addition of the substrate and inhibitor in reaction mixtures containing 50 mM CHES (pH 9.0) at 30 °C with 2.0 mM paraoxon as the substrate. The addition of paraoxon to a premixture of *Sb*-PTE (10 nM) and 1-butynyl dibutylphosphate (20 nM) resulted in a reaction rate that was 13% of the uninhibited control reaction rate. The addition of 1-
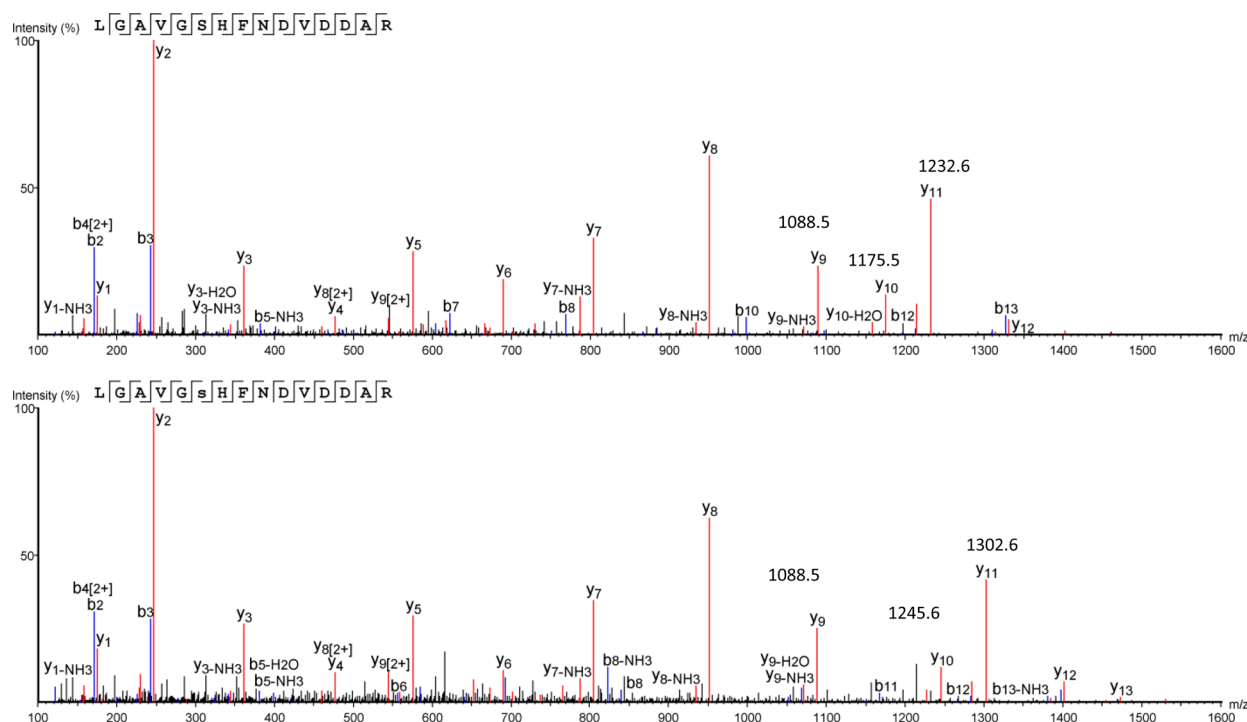
Figure 4. MS/MS of the peptide from residue Leu-469 to Arg-483 of *Sb*-PTE. The top panel shows the spectrum for the unmodified protein, while the bottom panel shows the protein after inactivation by 1-butynyl dibutylphosphate (**18**). Modification is identified at Ser-474 (peak y_{10}). Masses for peaks y_9–y_{11} are provided in the plot.

butynyl dibutylphosphate (20 nM) to a premixture of *Sb*-PTE (10 nM) and the substrate paraoxon (2.0 mM) gave a reaction rate that was 62% of the uninhibited control reaction rate. These data demonstrated that the substrate paraoxon (**1**) can protect *Sb*-PTE against inactivation by the suicide substrate 1-butynyl dibutylphosphate (**20**).

Construction of a Homology Model for *Sb*-Phosphotriesterase. A protein BLAST search of the nonredundant protein database revealed that *Sb*-PTE is most closely related to two proteins from *Sphingomonas echinoides* (WP_010408975, gi|498094819) and *Sphingomonas* sp. DC-2 (WP_030539984, gi|663820113) of unknown function and structure. The only proteins of known function that were identified were FedA from *Burkholderia* sp. NF100 (BAE86940, gi|89885659) and OphB from *Burkholderia* sp. JBA3 (ABP65302, gi|145388876). Both FedA and OphB have been reported to hydrolyze organophosphate insecticides.[28,29] The only protein of known structure identified was the surface antigen protein from *Methanosarcina mazei* (PDB entry 1L0Q) where the sequence of *Sb*-PTE aligned with the β-propeller domain of this protein.[30] The sequence of *Sb*-PTE was submitted to the Phyre2 and FFAS structure predictor servers, which use position specific iteration sequence alignment algorithms to identify potential template structures for homology models.[24,25] All of the highly rated protein templates were for seven-blade β-propellers. The highest rated template, which contained a complete β-propeller, was for the leptospiral antigen Lp49 protein (PDB entry 3BWS).[23]

Homology models were constructed using Phyre2 and FFAS. The model from Phyre2 is presented in Figure 5. Unfortunately, none of the identified template structures, including Lp49, have known functions or bind metals. However, two other β-propeller enzymes, squid DFPase (PDB entry 2GVW) and human PON1 (PDB entry 3SRG),
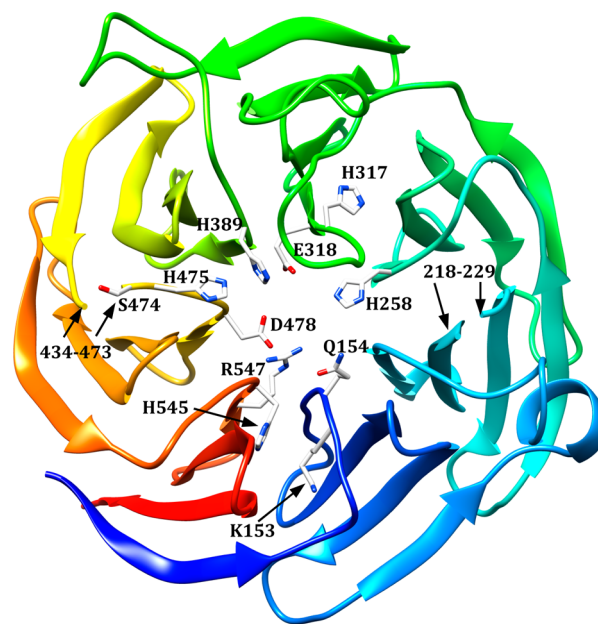

Figure 5. Homology model of *Sb*-PTE generated by Phyre2 based on the leptospiral antigen protein Lp49 (PDB entry 3BWS). Potential active site residues are labeled. The beginning and end of missing loops 218–229 and 434–473 are shown.

are well-known metal-dependent enzymes that can hydrolyze organophosphorus esters.[31,32] While PON1 and DFPase do not have conserved sequences, their six-blade propeller structures and catalytic metal binding sites are very similar. Despite being a six-blade rather than a seven-blade propeller protein, both PON1 and DFPase could be structurally aligned to the homology model of *Sb*-PTE. Comparison of the protein structure in the region of the catalytic metal binding sites of

DFPase and PON1 identified a set of potential metal binding residues in *Sb*-PTE. The best alignment was observed with the metal center contained within DFPase, where the *Sb*-PTE residues appear in approximately the same geometric orientation (Figure 6). In DFPase, the catalytic calcium is
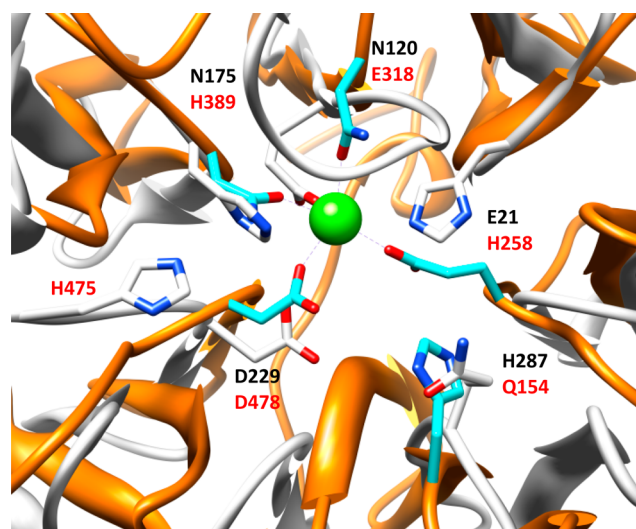

Figure 6. Structural alignment of the metal center of DFPase (PDB entry 2GVW) with the proposed homology model of *Sb*-PTE. Metal binding residues from DFPase (orange) are labeled in black, while residues from *Sb*-PTE (white) are labeled in red. Also shown are the active site base of DFPase (His-287) and a potential active site base in *Sb*-PTE (His-475).

ligated by Glu-21, Asn-120, Asn-175, and Asp-229. In *Sb*-PTE, these residues appear to be His-258, Glu-318, His-389, and Asp-478. In the catalytic mechanism of DFPase, Asp-229 is proposed to function as a nucleophile while His-287 is an active site base.[32] In *Sb*-PTE, the apparent active site aspartate is Asp-478, but the residue from *Sb*-PTE that is equivalent to His-287 in the homology model is Asn-154, which is unlikely to serve as a general acid/base. In the reaction mechanism of PON1, the active site base is proposed to be a His-115/His-134 dyad, which is found at a position structurally distinct from that in the active site of DFPase.[33] Similarly, in the homology model of *Sb*-PTE, His-475 is found within hydrogen bonding distance of the proposed metal binding residue His-389 and is positioned to function as an active site base.

Mutation of Potential Critical Amino Acid Residues. To gain insight into the active site of *Sb*-PTE, 14 site-directed mutants (K153Q, Q154A, Y219F, H258N, H317N, E318Q, H389N, Y456F, S458A, S474A, H475N, D478N, H545N, and R547Q) were constructed on the basis of the homology model of *Sb*-PTE and the residues that were labeled with the suicide substrate (Figure 5). Each of these variants was successfully expressed; the native metal was removed, and the apoenzymes were reconstituted with manganese. The kinetic parameters of the reconstituted variants with paraoxon are listed in Table 2. The mutation of His-389, Ser-474, His-475, and Lys-153 led to drastic decreases in catalytic activity. Mutation of His-258 and His-317 also reduced the activity of *Sb*-PTE by factors of 600 and 180, respectively, relative to that for the hydrolysis of paraoxon by wild-type *Sb*-PTE. Mutation of the putative metal ligands in the active site of *Sb*-PTE (His-389, Glu-318, His-258, and Asp-478) resulted in significant losses of catalytic activity. Lys-153 and His-317 are putatively situated in loops that form

Table 2. Kinetic Constants for Mutants of *Sb*-PTE with Paraoxon at pH 9.0 and 30 °C

substrate	k_{cat} (s^{-1})	K_m (mM)	k_{cat}/K_m (M^{-1} s^{-1})
wild-type	24.3 ± 0.5	0.18 ± 0.02	(1.4 ± 0.1) × 10^5
K153Q	nd^a	nd^a	(3.8 ± 0.2) × 10
Q154A	18.8 ± 0.1	0.62 ± 0.06	(1.7 ± 0.2) × 10^4
Y219F	1.43 ± 0.03	0.09 ± 0.01	(1.6 ± 0.2) × 10^4
H258N	0.20 ± 0.01	1.7 ± 0.1	(1.2 ± 0.1) × 10^2
H317N	0.24 ± 0.01	0.49 ± 0.05	(4.9 ± 0.5) × 10^2
E318Q	4.3 ± 0.1	0.19 ± 0.02	(2.3 ± 0.2) × 10^4
H389N	0.013 ± 0.001	1.6 ± 0.2	(8.1 ± 0.1) × 10^0
Y456F	33 ± 1	0.42 ± 0.04	(7.9 ± 0.8) × 10^4
S458A	26 ± 1	0.33 ± 0.04	(7.9 ± 0.8) × 10^4
S474A	0.014 ± 0.001	0.9 ± 0.1	(1.5 ± 0.1) × 10
H475N	0.042 ± 0.001	0.52 ± 0.07	(8 ± 1) × 10
D478N	2.10 ± 0.07	0.40 ± 0.04	(5.3 ± 0.6) × 10^3
H545N	1.5 ± 0.1	1.2 ± 0.1	(1.3 ± 0.2) × 10^3
R547Q	4.9 ± 0.2	0.24 ± 0.03	(2.0 ± 0.3) × 10^4

^{a}Not determined.

the central cavity inside the β-propeller. The D478N mutant has the highest value of k_{cat}/K_m (5 × 10^3 M^{-1} s^{-1}) among the four predicted metal ligand mutants. Metal analysis by ICP-MS demonstrated that the level of binding to manganese was most dramatically reduced by mutations to His-258, Glu-318, Ser-474, Asp-478, and His-545. Of the other variants analyzed, His-389 had a mild effect on manganese binding while the others had little to no apparent effect on metal binding.

DISCUSSION

Purification of *Sb*-PTE. As previously reported, *Sb*-PTE could be successfully expressed in *E. coli*.[10] Like the protein purified from the native species, the *E. coli*-expressed enzyme demonstrates a lower than expected molecular mass. While the gene sequence for *Sb*-PTE does not contain a common cleavage site for N-terminal processing in *E. coli*, the expressed enzyme was cleanly cleaved between Ser-87 and Gln-88.[34] Multiple attempts to express *Sb*-PTE directly as an N-terminal truncate resulted in insoluble protein with no catalytic activity. Interestingly, the Lp49 protein, upon which the homology model of *Sb*-PTE was based, contains an N-terminal β-sandwich domain that packs against the first strand of the β-propeller domain.[23] It is known that in many multidomain proteins, the folding of an N-terminal domain can stabilize the folding of subsequent protein domains.[35] While the underlying mechanism of cleavage remains unclear, the expression of *Sb*-PTE suggests that it may be initially expressed as a proenzyme with an N-terminal domain that is required for proper folding.

The enzymatic activity of *Sb*-PTE is dependent on metal ions with the best activity being observed with manganese. Maximal catalytic activity was achieved with the addition of 1.0 mM MnCl$_2$ in kinetic assays. Similar weak binding of the catalytic metal has been reported for the β-propeller enzyme PON1.[36] Chelation of the metal ions resulted in complete attenuation of the enzymatic activity, while reconstitution results in full catalytic activity.

Catalytic Activity. *Sb*-PTE was previously reported to hydrolyze a variety of organophosphorus triesters, although the catalytic activity was only quantified as the fraction of the substrate hydrolyzed in 30 min.[10] The kinetic characterization of the enzymatic activity has now allowed for a more complete comparison to other phosphotriesterases. The activity of *Sb*-

PTE with the substrate paraoxon is diminished more than 2 orders of magnitude below that observed with *Pd*-PTE, but the catalytic activity of *Pd*-PTE is strongly dependent on the pK_a of the leaving group (β value ~ −2).[7] The activity of *Pd*-PTE is reduced by ~6 orders of magnitude for the cleavage of an unactivated phenol leaving group.[7] The activity of *Sb*-PTE does not show this strong dependence on the pK_a of the leaving group and is diminished <2-fold using an unactivated phenol leaving group in comparison with a *p*-nitrophenyl leaving group. This suggests that the mechanism for the protonation of the leaving group is quite different between the two proteins.

While *Pd*-PTE is well-known for its broad substrate specificity, *Sb*-PTE appears to be able to hydrolyze many compounds that *Pd*-PTE cannot hydrolyze, including various plasticizers, flame retardants, and solvents.[4−9,37] The best activity of *Sb*-PTE was with the flame retardant triphenylphosphate (**8**), and this enzyme can also catalyze the hydrolysis of tris(2-chloroethyl) phosphate (**5**) and the "Aviation Sickness"-related compound, tricresol phosphate (**9**).[38] Quite remarkably, *Sb*-PTE can also hydrolyze phosphotriesters with a simple straight chain alcohol and thiol leaving groups, including tributyl phosphate (**7**), a solvent in nuclear fuel processing, and tribufos (**16**), a plant defoliant used in cotton harvesting, further suggesting that the mechanism for substrate hydrolysis exhibited by *Sb*-PTE will be significantly different from that of *Pd*-PTE.[39,40]

Homology Model of *Sb*-PTE. There is no structural information available for *Sb*-PTE or close homologues, but a homology model for *Sb*-PTE was constructed using the Phyre structure prediction server.[25] The model is based on the seven-blade β-propeller domain of the Lp49 antigen protein.[23] Structural alignment with the six-blade β-propeller DFPase suggests that *Sb*-PTE may bind metal ions in a similar manner, with the metal ligands being His-258, Glu-318, His-389, and Asp-478.[32] In squid DFPase, the active site base is His-287. In the *Sb*-PTE model, the equivalent residue is Gln-154, which cannot serve as a proton acceptor. The mutation of Gln-154 to an alanine residue resulted in a higher value of K_m for the hydrolysis of paraoxon but did not significantly alter the value of k_{cat}, further suggesting that Gln-154 is not an active site base. While the metal binding site is conserved between DFPase and PON1, the active site bases are located on the opposite side of the active site.[33] Similarly, His-475 of *Sb*-PTE appears to be appropriately positioned to participate in catalysis. Mutation of this residue to asparagine results in a value of k_{cat} that is reduced by 4 orders of magnitude, suggesting that His-475 may be the active site base.

To test the proposed metal binding residues, His-258, Glu-318, His-389, Asp-478, and additional potential ligands shown in the homology model (Lys-153, His-317, His-545, and Arg-547) were mutated to asparagine or glutamine. Three of the proposed metal binding residues (His-258, Glu-318, and Asp-478) showed moderate loss of activity in assays supplemented with excess manganese. Metal analysis of the reconstituted variants showed that their ability to bind manganese was severely diminished. The fourth mutant, H389N, showed a >3 order of magnitude loss in the value of k_{cat}. With this mutant, the level of binding of Mn^{2+} was decreased but not to the extent of the other proposed metal ligands. Of the other resides predicted to be in the vicinity of the metal site, K153Q, H317N, and R547Q exhibited diminished catalytic activity, but the binding of manganese did not appear to be greatly affected. By contrast, H545N shows a moderate loss of activity but severely

weakened binding of manganese. The value of k_{cat} is similar to those of the mutants for the other proposed metal binding ligands. These results suggest that His-545 rather than His-389 may be the fourth metal binding ligand and that His-389 may be acting in concert with His-475 as an active site dyad to deprotonate water and protonate the leaving group of the substrate. The determination of the three-dimensional structure of *Sb*-PTE is in progress.

Covalent Modification of Active Site Residues. The inhibitor 1-butynyl dibutylphosphate (**20**) proved to be an incredibly potent inhibitor of *Sb*-PTE. Full inhibition was observed with approximately 2 equiv of inhibitor. By contrast, *Pd*-PTE was reported to hydrolyze ~500 molecules of a similar mechanism-based inhibitor before being fully inactivated.[41] The ability to reactivate *Sb*-PTE with hydroxylamine following inactivation with 1-butynyl dibutylphosphate (**20**) suggests the loss of catalytic activity is most likely due to the modification of one or more histidine residues.[41,42] However, MS/MS analysis identified two serine residues (Ser-458 and Ser-474) and two tyrosine residues (Tyr-219 and Tyr-456) as being labeled. The labeling of tyrosine and serine may have occurred by migration of the label from the original site of histidine labeling. Unfortunately, Tyr-219, Ser-458, and Tyr-456 were not localized in the homology model, but they are likely positioned on loops that are positioned above the proposed active site. Mutation of these resides did not result in substantial loss of catalytic activity or metal binding. Mutation of Ser-474, which appears to be adjacent to His-475 (the proposed active site base), did severely diminish the activity of *Sb*-PTE. Despite not being able to capture the critical histidine residue, all of the identified residues appear to be at positions that support the location of the proposed active site.

Metal Center and Mechanism of Action. The proposed metal binding site of *Sb*-PTE contains two histidine ligands, an aspartate and a glutamate, which appear to coordinate a single manganese ion. Similar combinations of histidine and carboxylate ligands are seen in mononuclear manganese enzymes such as superoxide dismutase and oxalate decarboxylase.[43,44] The enzymes L-ribulose 3-epimerase and D-tagatose 3-epimerase both contain a metal binding site with three carboxylate residues and one histidine residue,[45,46] while L-arabinose isomerase contains a two-histidine, two-carboxylate motif similar to the proposed site in *Sb*-PTE. However, none of these other single-manganese enzymes is known to activate water for hydrolytic attack. Numerous examples are known for manganese-containing hydrolases, but they contain binuclear metal centers to activate water.[47−50] The single metal binding site appears to make *Sb*-PTE unique among manganese-containing hydrolases.

Numerous phosphotriesterase enzymes have been characterized, but the only known examples able to utilize a single metal ion for catalysis are the β-propeller enzymes DFPase and PON1.[31,32] DFPase is thought to achieve this by utilizing covalent catalysis where the metal binding residue Asp-229 serves as the attacking nucleophile.[32] Covalent catalysis has not been definitively demonstrated for PON1, but it is also suggested to go through a mechanism similar to that of DFPase with phosphotriester substrates.[31,32] The hydrolysis of lactone substrates by PON1 is thought to proceed via a noncovalent mechanism, suggesting a direct attack by water could be also be possible for this enzyme. The proposed structure of *Sb*-PTE has Asp-478 in a position equivalent to that of the nucleophilic aspartate residue in DFPase, and thus, this enzyme may

proceed through a similar covalent reaction mechanism. Alternatively, His-475 and His-389 may be acting in conjunction with Asp-478 to provide a catalytic triad with sufficient ability to deprotonate an attacking water and protonate the leaving group, allowing the direct attack of water even with poor substrates. The question of a covalent versus direct attack by water, can be answered by the utilization of chiral thiophosphate substrates.[51] These experiments are underway for *Sb*-PTE.

Potential Applications. There is mounting concern about the environmental impact of the use of organophosphorus flame retardants in plastics and foam materials as well as concerns about organophosphorus solvents used industrially. Many of these compounds are known or suspected carcinogens and are being produced at rates of millions of tons per year.[2,3] Aviation Syndrome has been directly linked to the use of tricresol phosphate (**9**) in jet fuel and lubricants.[38] Unlike insecticides, these compounds are intended to function under the harsh conditions of combustion and consequently are very stable. Typical phosphotriester enzymes have no activity against these compounds because of the lack of a sufficiently labile leaving group. *Sb*-PTE may prove to be useful for the environmental remediation of these compounds because of its unique ability to hydrolyze phosphotriesters without an activated leaving group.

■ AUTHOR INFORMATION

Corresponding Author

*Telephone: 979-845-3373. E-mail: raushel@tamu.edu. Fax: 979-845-9452.

Present Address

§H.X., K.G.H., and D.R.: Department of Chemistry and Biochemistry, 101 Bagby Ave., Baylor University, Waco, TX 76798-7348.

Notes

The authors declare no competing financial interest.

■ ABBREVIATIONS

Pd-PTE, phosphotriesterase from *P. diminuta*; *Sm*-PTE, phosphotriesterase from *Sphingomonas* sp. strain TDK1; *Sb*-PTE, phosphotriesterase from *Sphingobium* sp. strain TCM1

■ REFERENCES

(1) Maxwell, D. M., Brecht, K. M., Koplovitz, I., and Sweeney, R. E. (2006) Acetylcholinesterase inhibition: does it explain the toxicity of organophosphorus compounds? *Arch. Toxicol. 80*, 756−760.

(2) Reemtsma, T., Quintana, J. B., Rodil, R., Garcia-Lopez, M., and Rodriguez, I. (2008) Organophosphorus flame retardants and plasticizers in water and air I. Occurrence and fate. *TrAC, Trends Anal. Chem. 27*, 727−737.

(3) van der Veen, I., and de Boer, J. (2012) Phosphorus flame retardants: properties, production, environmental occurrence, toxicity and analysis. *Chemosphere 88*, 1119−1153.

(4) Cherny, I., Greisen, P., Jr., Ashani, Y., Khare, S. D., Oberdorfer, G., Leader, H., Baker, D., and Tawfik, D. S. (2013) Engineering V-type nerve agents detoxifying enzymes using computationally focused libraries. *ACS Chem. Biol. 8*, 2394−2403.

(5) Dawson, R. M., Pantelidis, S., Rose, H. R., and Kotsonis, S. E. (2008) Degradation of nerve agents by an organophosphate-degrading agent (OpdA). *J. Hazard. Mater. 157*, 308−314.

(6) Dumas, D. P., Caldwell, S. R., Wild, J. R., and Raushel, F. M. (1989) Purification and properties of the phosphotriesterase from *Pseudomonas diminuta*. *J. Biol. Chem. 264*, 19659−19665.

(7) Hong, S. B., and Raushel, F. M. (1996) Metal-substrate interactions facilitate the catalytic activity of the bacterial phosphotriesterase. *Biochemistry 35*, 10904−10912.

(8) Tsai, P. C., Fox, N., Bigley, A. N., Harvey, S. P., Barondeau, D. P., and Raushel, F. M. (2012) Enzymes for the homeland defense: optimizing phosphotriesterase for the hydrolysis of organophosphate nerve agents. *Biochemistry 51*, 6463−6475.

(9) Yang, H., Carr, P. D., McLoughlin, S. Y., Liu, J. W., Horne, I., Qiu, X., Jeffries, C. M., Russell, R. J., Oakeshott, J. G., and Ollis, D. L. (2003) Evolution of an organophosphate-degrading enzyme: a comparison of natural and directed evolution. *Protein Eng., Des. Sel. 16*, 135−145.

(10) Abe, K., Yoshida, S., Suzuki, Y., Mori, J., Doi, Y., Takahashi, S., and Kera, Y. (2014) Haloalkylphosphorus hydrolases purified from *Sphingomonas* sp. strain TDK1 and *Sphingobium* sp. strain TCM1. *Appl. Environ. Microbiol. 80*, 5866−5873.

(11) Chen-Goodspeed, M., Sogorb, M. A., Wu, F., Hong, S. B., and Raushel, F. M. (2001) Structural determinants of the substrate and stereochemical specificity of phosphotriesterase. *Biochemistry 40*, 1325−1331.

(12) Law, K. S., Acey, R. A., Smith, C. R., Benton, D. A., Soroushian, S., Eckenrod, B., Stedman, R., Kantardjieff, K. A., and Nakayama, K. (2007) Dialkyl phenyl phosphates as novel selective inhibitors of butyrylcholinesterase. *Biochem. Biophys. Res. Commun. 355*, 371−378.

(13) Bigley, A. N., Xu, C., Henderson, T. J., Harvey, S. P., and Raushel, F. M. (2013) Enzymatic neutralization of the chemical warfare agent VX: evolution of phosphotriesterase for phosphorothiolate hydrolysis. *J. Am. Chem. Soc. 135*, 10426−10432.

(14) Chapman, E., and Wong, C. H. (2002) A pH sensitive colorometric assay for the high-throughput screening of enzyme inhibitors and substrates: a case study using kinases. *Bioorg. Med. Chem. 10*, 551−555.

(15) Xiang, D. F., Kolb, P., Fedorov, A. A., Meier, M. M., Fedorov, L. V., Nguyen, T. T., Sterner, R., Almo, S. C., Shoichet, B. K., and Raushel, F. M. (2009) Functional annotation and three-dimensional structure of Dr0930 from *Deinococcus radiodurans*, a close relative of phosphotriesterase in the amidohydrolase superfamily. *Biochemistry 48*, 2237−2247.

(16) Michaelis, L., and Menten, M. L. (1913) Die Kinetik der Invertinwirkung. *Biochemische Zeitschrift 49*, 333−369.

(17) Mlotkowska, B., and Wartalowskagraczyk, M. (1987) Direct conversion of alcohols into phosphorothiolates. *J. Prakt. Chem. 329*, 735−740.

(18) Santschi, N., and Togni, A. (2011) Electrophilic trifluoromethylation of S-hydrogen phosphorothioates. *J. Org. Chem. 76*, 4189−4193.

(19) Stang, P. J., Kitamura, T., Boehshar, M., and Wingert, H. (1989) Acetylenic esters - preparation and characterization of alkynyl dialkyl phosphates, RC = COPO(OR′)₂. *J. Am. Chem. Soc. 111*, 2225−2230.

(20) Havare, N., and Plattner, D. A. (2012) Oxidative cleavage of alpha-aryl aldehydes using iodosylbenzene. *Org. Lett. 14*, 5078−5081.

(21) Smith, N. D., Kahraman, M., Govek, S. P., Nagasawa, J. Y., and Lai, A. G. (2012) Estrogen receptor modulators and use thereof. U.K. Patent Application GB 2,483,736 (A).

(22) Shevchenko, A., Tomas, H., Havlis, J., Olsen, J. V., and Mann, M. (2007) In-gel digestion for mass spectrometric characterization of proteins and proteomes. *Nat. Protoc. 1*, 2856−2860.

(23) Giuseppe, P. O., Neves, F. O., Nascimento, A. L., and Guimaraes, B. G. (2008) The leptospiral antigen Lp49 is a two-domain protein with putative protein binding function. *J. Struct. Biol. 163*, 53−60.

(24) Jaroszewski, L., Li, Z., Cai, X. H., Weber, C., and Godzik, A. (2011) FFAS server: novel features and applications. *Nucleic Acids Res. 39*, W38−44.

(25) Kelley, L. A., and Sternberg, M. J. (2009) Protein structure prediction on the Web: a case study using the Phyre server. *Nat. Protoc. 4*, 363−371.

(26) Pettersen, E. F., Goddard, T. D., Huang, C. C., Couch, G. S., Greenblatt, D. M., Meng, E. C., and Ferrin, T. E. (2004) UCSF Chimera–a visualization system for exploratory research and analysis. *J. Comput. Chem. 25*, 1605−1612.

(27) Silverman, R. B. (1988) *Mechanism Based Enzyme Inactivation: Chemistry and Enzymology*, Vol. 1, CRC Press, Boca Raton, FL.

(28) Kim, T., Ahn, J. H., Choi, M. K., Weon, H. Y., Kim, M. S., Seong, C. N., Song, H. G., and Ka, J. O. (2007) Cloning and expression of a parathion hydrolase gene from a soil bacterium, *Burkholderia* sp. JBA3. *J. Microbiol. Biotechnol. 17*, 1890−1893.

(29) Tago, K., Yonezawa, S., Ohkouchi, T., Hashimoto, M., and Hayatsu, M. (2006) Purification and characterization of fenitrothion hydrolase from *Burkholderia* sp. NF100. *J. Biosci. Bioeng. 101*, 80−82.

(30) Jing, H., Takagi, J., Liu, J. H., Lindgren, S., Zhang, R. G., Joachimiak, A., Wang, J. H., and Springer, T. A. (2002) Archaeal surface layer proteins contain beta propeller, PKD, and beta helix domains and are related to metazoan cell surface proteins. *Structure 10*, 1453−1464.

(31) Ben-David, M., Elias, M., Filippi, J. J., Dunach, E., Silman, I., Sussman, J. L., and Tawfik, D. S. (2012) Catalytic versatility and backups in enzyme active sites: the case of serum paraoxonase 1. *J. Mol. Biol. 418*, 181−196.

(32) Blum, M. M., Lohr, F., Richardt, A., Ruterjans, H., and Chen, J. C. (2006) Binding of a designed substrate analogue to diisopropyl fluorophosphatase: implications for the phosphotriesterase mechanism. *J. Am. Chem. Soc. 128*, 12750−12757.

(33) Khersonsky, O., and Tawfik, D. S. (2006) The histidine 115-histidine 134 dyad mediates the lactonase activity of mammalian serum paraoxonases. *J. Biol. Chem. 281*, 7649−7656.

(34) Choo, K. H., and Ranganathan, S. (2008) Flanking signal and mature peptide residues influence signal peptide cleavage. *BMC Bioinf. 9*, S15.

(35) Choi, S. I., Son, A., Lim, K. H., Jeong, H., and Seong, B. L. (2012) Macromolecule-assisted *de novo* protein folding. *Int. J. Mol. Sci. 13*, 10368−10386.

(36) Kuo, C. L., and La Du, B. N. (1995) Comparison of purified human and rabbit serum paraoxonases. *Drug Metab. Dispos. 23*, 935−944.

(37) Nowlan, C., Li, Y., Hermann, J. C., Evans, T., Carpenter, J., Ghanem, E., Shoichet, B. K., and Raushel, F. M. (2006) Resolution of chiral phosphate, phosphonate, and phosphinate esters by an enantioselective enzyme library. *J. Am. Chem. Soc. 128*, 15892−15902.

(38) Mackerer, C. R., Barth, M. L., Krueger, A. J., Chawla, B., and Roy, T. A. (1999) Comparison of neurotoxic effects and potential risks from oral administration or ingestion of tricresyl phosphate and jet engine oil containing tricresyl phosphate. *J. Toxicol. Environ. Health, Part A 57*, 293−328.

(39) Nakamura, A. (1991) *International programme on chemical safety-environmental heath criteria 112-tri-n-butyl phosphate*; World Health Organizaiton, Geneva.

(40) Potter, T. L., Truman, C. C., Bosch, D. D., and Bednarz, C. W. (2003) Cotton defoliant runoff as a function of active ingredient and tillage. *J. Environ. Qual. 32*, 2180−2188.

(41) Banzon, J. A., Kuo, J. M., Miles, B. W., Fischer, D. R., Stang, P. J., and Raushel, F. M. (1995) Mechanism-based inactivation of phosphotriesterase by reaction of a critical histidine with a ketene intermediate. *Biochemistry 34*, 743−749.

(42) Fife, T. H. (1965) Steric Effects in hydrolysis of N-acylimidazoles and esters of p-nitrophenol. *J. Am. Chem. Soc. 87*, 4597−4604.

(43) Dennis, R. J., Micossi, E., McCarthy, J., Moe, E., Gordon, E. J., Kozielski-Stuhrmann, S., Leonard, G. A., and McSweeney, S. (2006) Structure of the manganese superoxide dismutase from Deinococcus radiodurans in two crystal forms. *Acta Crystallogr., Sect. F: Struct. Biol. Cryst. Commun. 62*, 325−329.

(44) Just, V. J., Stevenson, C. E., Bowater, L., Tanner, A., Lawson, D. M., and Bornemann, S. (2004) A closed conformation of Bacillus subtilis oxalate decarboxylase OxdC provides evidence for the true identity of the active site. *J. Biol. Chem. 279*, 19867−19874.

(45) Uechi, K., Sakuraba, H., Yoshihara, A., Morimoto, K., and Takata, G. (2013) Structural insight into L-ribulose 3-epimerase from *Mesorhizobium loti*. *Acta Crystallogr., Sect. D: Biol. Crystallogr. 69*, 2330−2339.

(46) Yoshida, H., Yamada, M., Nishitani, T., Takada, G., Izumori, K., and Kamitori, S. (2007) Crystal structures of D-tagatose 3-epimerase from *Pseudomonas cichorii* and its complexes with D-tagatose and D-fructose. *J. Mol. Biol. 374*, 443−453.

(47) Gajadeera, C. S., Zhang, X., Wei, Y., and Tsodikov, O. V. (2015) Structure of inorganic pyrophosphatase from Staphylococcus aureus reveals conformational flexibility of the active site. *J. Struct. Biol. 189*, 81−86.

(48) Huguet, F., Melet, A., Alves de Sousa, R., Lieutaud, A., Chevalier, J., Maigre, L., Deschamps, P., Tomas, A., Leulliot, N., Pages, J. M., and Artaud, I. (2012) Hydroxamic acids as potent inhibitors of Fe(II) and Mn(II) *E. coli* methionine aminopeptidase: biological activities and X-ray structures of oxazole hydroxamate-EcMetAP-Mn complexes. *ChemMedChem 7*, 1020−1030.

(49) Lee, S. J., Kim do, J., Kim, H. S., Lee, B. I., Yoon, H. J., Yoon, J. Y., Kim, K. H., Jang, J. Y., Im, H. N., An, D. R., Song, J. S., Kim, H.-J., and Suh, S. W. (2011) Crystal structures of *Pseudomonas aeruginosa* guanidinobutyrase and guanidinopropionase, members of the ureohydrolase superfamily. *J. Struct. Biol. 175*, 329−338.

(50) Stepankova, A., Duskova, J., Skalova, T., Hasek, J., Koval, T., Østergaard, L. H., and Dohnalek, J. (2013) Organophosphorus acid anhydrolase from *Alteromonas macleodii*: structural study and functional relationship to prolidases. *Acta Crystallogr., Sect. F: Struct. Biol. Cryst. Commun. 69*, 346−354.

(51) Lewis, V. E., Donarski, W. J., Wild, J. R., and Raushel, F. M. (1988) Mechanism and stereochemical course at phosphorus of the reaction catalyzed by a bacterial phosphotriesterase. *Biochemistry 27*, 1591−1597.